J|A|C|S
ARTICLES

Layer-by-Layer Assembly of Polyelectrolytes into Ionic Current Rectifying Solid-State Nanopores: Insights from Theory and Experiment

Mubarak Ali,[†] Basit Yameen,[‡] Javier Cervera,[§] Patricio Ramírez,[||]
Reinhard Neumann,[⊥] Wolfgang Ensinger,[†] Wolfgang Knoll,[#] and Omar Azzaroni*,[∇]

Fachbereich Material-u. Geowissenschaften, Fachgebiet Materialanalytik, Technische Universität Darmstadt, Petersenstrasse 23, D-64287 Darmstadt, Germany, Max-Planck-Institut für Polymerforschung, Ackermannweg 10, 55128 Mainz, Germany, Departament de Física de la Terra i Termodinámica, Universitat de Valéncia, E-46100 Burjassot, Spain, Departament de Física Aplicada, Universidad Politécnica de Valencia, E-46022 Valencia, Spain, GSI Helmholtzzentrum für Schwerionenforschung GmbH, Planckstrasse 1, D-64291 Darmstadt, Germany, Austrian Institute of Technology, Donau-City-Strasse 1, 1220 Vienna, Austria, and Instituto de Investigaciones Fisicoquímicas Teóricas y Aplicadas (INIFTA), Depto. de Química, Fac. de Ciencias Exactas, Universidad Nacional de La Plata, CONICET, CC 16 Suc.4 (1900) La Plata, Argentina

Received February 4, 2010; E-mail: azzaroni@inifta.unlp.edu.ar

Abstract: Molecular design of ionic current rectifiers created on the basis of single conical nanopores is receiving increasing attention by the scientific community. Part of the appeal of this topic relies on the interest in sensors and fluidic nanoactuators based on the transport of ions and molecules through nanopore architectures that can readily be integrated into functional systems. The chemical modification of the pore walls controls not only the diameter of these nanoarchitectures but also their selectivity and transport properties. In order to confer selectivity to solid-state nanopores, it is necessary to develop and explore new methods for functionalizing the pore walls. Hence, the creation of functional nanopores capable of acting as selective ion channels or smart nanofluidic sensors depends critically on our ability to assemble and build up molecular architectures in a predictable manner within confined geometries with dimensions comparable to the size of the building blocks themselves. In this context, layer-by-layer deposition of polyelectrolytes offers a straightforward process for creating nanoscopic supramolecular assemblies displaying a wide variety of functional features. In this work, we describe for the first time the integration of layer-by-layer polyelectrolyte assemblies into single conical nanopores in order to study and explore the functional features arising from the creation of charged supramolecular assemblies within the constrained geometry of the nanofluidic device. To address this challenging topic, we used a combined experimental and theoretical approach to elucidate and quantify the electrostatic changes taking place inside the nanopore during the supramolecular assembly process. The multilayered films were built up through consecutive layer-by-layer adsorption of poly(allylamine hydrochloride) (PAH) and poly(styrenesulfonate) (PSS) on the pore surface. Our results show that the charge transport properties of single conical nanopores functionalized with PAH/PSS assemblies are highly dependent on the number of layers assembled on the pore wall. In contrast to what happens with PAH/PSS films deposited on planar surfaces (quantitative charge reversal), the surface charge of the pore walls decreases dramatically with the number of PAH/PSS layers assembled into the nanopore. This behavior was attributed to the nanoconfinement-induced structural reorganization of the polyelectrolyte layers, leading to the efficient formation of ion pairs and promoting a marked decrease in the net fixed charges on the nanopore walls. We consider that these results are of paramount relevance for the modification of nanopores, nanopipets, and nanoelectrodes using charged supramolecular assemblies, as well as of importance in "soft nanotechnology" provided that structural complexity, induced by nanoconfinement, can define the functional properties of self-assembled polymeric nanostructures.

Introduction

As we move further into the new century, nanotechnology seems indeed to offer almost unlimited opportunities for fundamental and applied science. The virtues of working with nanofluidic elements are being increasingly recognized by the scientific community as well as by the technological world.[1−18] This has led to the emergence of a research area that is currently at the forefront of materials science and engineering. The blend of tools and concepts from different disciplines has resulted in an increasing mastery in construction of nanoscale fluidic structures.[19−23] For instance, the advent of track-etching techniques has given a decisive impetus not only to the development of this exciting area of nanotechnology but also opened up new possibilities to reproducibly engineer nanopore and nanochannel architectures with various shapes and diameters down to a few nanometers.[24−27] This endeavor gave rise to design concepts to construct fully "abiotic" inorganic and polymeric nanochan-

---

[†] Technische Universität Darmstadt.
[‡] Max-Planck-Institut für Polymerforschung.
[§] Universitat de Valéncia.
[||] Universidad Politécnica de Valencia.
[⊥] GSI Helmholtzzentrum für Schwerionenforschung GmbH.
[#] Austrian Institute of Technology.
[∇] Universidad Nacional de La Plata (http://softmatter.quimica.unlp.edu.ar).

nels with dimensions comparable to those of biological molecules. One major attraction of these nanofluidic elements is their outstanding ability to control and manipulate the transport of chemical and biochemical species flowing through them, thus enabling the construction of ionic circuits capable of sensing, switching, or separating diverse species in aqueous solutions.[11,17,21,28] Furthermore, these nanofluidic devices have also been shown to display transport properties that resemble biological protein ion channels, such as ion selectivity, current rectification, flux inhibition by protons and divalent cations, transport of ions against concentration gradients, and even ion current fluctuations.[29−35] In the particular case of asymmetric nanochannels/nanopores, appealing effects arise when the channel surface is charged and the dimensions are comparable to the Debye length. A spatial change in the effect of surface charge along the length of a channel results in ionic concentration enhancement and depletion as well as in generation of space charge.[36−38] As a consequence, this effect arising from asymmetric geometries in uniformly surface charged nanochannels results in rectification of ionic current that mimics biological ion channels.[39] These fascinating physicochemical properties displayed by charged asymmetric nanochannels or nanopores provided the scenario to create new functional and addressable nanofluidic architectures and also led to the birth of a whole

new area of research concerning the design of nanochannel-based devices resting on surface charge governed ionic transport.[40] Benchmark examples are recently developed nanofluidic or bipolar ionic diodes displaying accurately controlled transport properties.[41,42]

The central feature that determines the rectifying characteristics of asymmetric nanopores is the nanoscale control over the surface properties of the pore walls.[43] However, controlling the internal architecture and the chemical features of synthetic nanopores as precisely as nature does in biological channels is a nontrivial task. As a consequence, finding new, simple, and straightforward strategies to manipulate the surface charges of conical nanopores is of paramount importance to further expand the potentialities of these nanosized architectures. To the best of our knowledge, the tailoring of surface charges in single asymmetric nanopores has been exclusively performed using monolayer and brush assemblies.[2,5,9,10,18,20,39,41,44−50] Within this framework, we should highlight that the layer-by-layer (LbL) assembly of polyelectrolytes represents a versatile method to build up nanoscale functional thin films,[51−55] even in nanoconstrained geometries.[56] Layer-by-layer growth provides access to the construction of nanoscopic functional multilayer systems with outstandingly high precision and is gaining increasing attention as a tool to build up supramolecular

(1) Hou, X.; Jiang, L. *ACS Nano* **2009**, *3*, 3339–3342.
(2) Harrell, C. C.; Kohli, P.; Siwy, Z.; Martin, C. R. *J. Am. Chem. Soc.* **2004**, *126*, 15646–15647.
(3) Sexton, L. T.; Horne, L. P.; Martin, C. R. *Mol. BioSyst.* **2007**, *3*, 667–685.
(4) Sexton, L. T.; Horne, L. P.; Sherrill, S. A.; Bishop, G. W.; Baker, L. A.; Martin, C. R. *J. Am. Chem. Soc.* **2007**, *129*, 13144–13152.
(5) Siwy, Z.; Trofin, L.; Kohli, P.; Baker, L. A.; Trautmann, C.; Martin, C. R. *J. Am. Chem. Soc.* **2005**, *127*, 5000–5001.
(6) Kosinska, I. D.; Goychuk, I.; Kostur, M.; Schmid, G.; Hänggi, P. *Phys. Rev. E* **2008**, *77*, 031131.
(7) Ali, M.; Yameen, B.; Neumann, R.; Ensinger, W.; Knoll, W.; Azzaroni, O. *J. Am. Chem. Soc.* **2008**, *130*, 16351–16358.
(8) van der Heyden, F. H. J.; Bonthuis, D. J.; Stein, D.; Meyer, C.; Dekker, C. *Nano Lett.* **2007**, *7*, 1022–1025.
(9) Karnik, R.; Fan, R.; Yue, M.; Li, D.; Yang, P.; Majumdar, A. *Nano Lett.* **2005**, *5*, 943–948.
(10) Daiguji, H.; Yang, P.; Majumdar, A. *Nano Lett.* **2004**, *4*, 137–142.
(11) Howorka, S.; Zuzanna Siwy, Z. *Chem. Soc. Rev.* **2009**, *38*, 2360–2384.
(12) He, Y.; Gillespie, D.; Boda, D.; Vlassiouk, I.; Eisenberg, R. S.; Siwy, Z. S. *J. Am. Chem. Soc.* **2009**, *131*, 5194–5202.
(13) Constantin, D.; Siwy, Z. S. *Phys. Rev. E* **2007**, *76*, 041202.
(14) Plecis, A.; Schoch, R. B.; Renaudv, P. *Nano Lett.* **2005**, *5*, 1147–1155.
(15) Ho, C.; Qiao, R.; Heng, J. B.; Chatterjeet, A.; Timp, R. J.; Alurut, N. R.; Timp, G. *Proc. Natl. Acad. Sci. U.S.A.* **2005**, *102*, 10445–10450.
(16) Liu, Q.; Wang, Y.; Guo, W.; Ji, H.; Xue, J.; Ouyang, Q. *Phys. Rev. E* **2007**, *75*, 051201.
(17) Dekker, C. *Nat. Nanotechnol.* **2007**, *2*, 209–215.
(18) Fan, R.; Yue, M.; Karnik, R.; Majumdar, A.; Yang, P. *Phys. Rev. Lett.* **2005**, *95*, 086607.
(19) Schoch, R. B.; Han, J.; Renaud, P. *Rev. Mod. Phys.* **2008**, *80*, 839–883.
(20) Karnik, R.; Duan, C.; Castelino, K.; Daiguji, H.; Majumdar, A. *Nano Lett.* **2007**, *7*, 547–551.
(21) Siwy, Z. S. *Adv. Funct. Mater.* **2006**, *16*, 735–746.
(22) Siwy, Z. S.; Martin, C. R. *Lect. Notes Phys.* **2007**, *711*, 349–365.
(23) Martin, C. R.; Siwy, Z. S. *Science* **2007**, *317*, 331–332.
(24) Spohr, R. *Radiat. Meas.* **2005**, *40*, 191–202.
(25) Schiedt, B.; Healy, K.; Morrison, A. P.; Neumann, R.; Siwy, Z. *Nucl. Instrum. Methods Phys. Res. B* **2005**, *236*, 109–116.
(26) Siwy, Z.; Apel, P.; Baur, D.; Dobrev, D. D.; Korchev, Y. E.; Neumann, R.; Spohr, R.; Trautmann, C.; Voss, K.-O. *Surf. Sci.* **2003**, *532−535*, 1061–1066.
(27) Apel, P. Y.; Korchev, Y. E.; Siwy, Z.; Spohr, R.; Yoshida, M. *Nucl. Instrum. Methods Phys. Res. B* **2001**, *184*, 337–346.
(28) Choi, Y.; Baker, L. A.; Hillebrenner, H.; Martin, C. R. *Phys. Chem. Chem. Phys.* **2006**, *8*, 4976–4988.
(29) Kalman, E.; Healy, K.; Siwy, Z. S. *Europhys. Lett.* **2007**, *78*, 28002.
(30) Siwy, Z. S.; Powell, M. R.; Petrov, A.; Kalman, E.; Trautmann, C.; Eisenberg, R. S. *Nano Lett.* **2006**, *6*, 1729–1734.
(31) Bashford, C. L. *Eur. Biophys. J.* **2004**, *33*, 280–282.
(32) Vlassiouk, I.; Smirnov, S.; Siwy, Z. *Nano Lett.* **2008**, *8*, 1978–1985.
(33) Siwy, Z.; Gu, Y.; Spohr, H. A.; Baur, D.; Wolf-Reber, A.; Spohr, R.; Apel, P.; Korchev, Y. E. *Europhys. Lett.* **2002**, *60*, 349–355.
(34) Lev, A. A.; Korchev, Y. E.; Rostovtseva, T. K.; Bashford, C. L.; Edmonds, D. T.; Pasternak, C. A. *Proc. R. Soc. London, Ser. B* **1993**, *252*, 187–192.
(35) Siwy, Z.; Fulinski, A. *Am. J. Phys.* **2004**, *72*, 567–574.
(36) Cervera, J.; Alcaraz, A.; Schiedt, B.; Neumann, R.; Ramírez, P. *J. Phys. Chem. C* **2007**, *111*, 12265–12273.
(37) Cervera, J.; Schiedt, B.; Neumann, R.; Mafé, S.; Ramírez, P. *J. Chem. Phys.* **2006**, *104*, 104706.
(38) Siwy, Z.; Fulinski, A. *Phys. Rev. Lett.* **2002**, *89*, 198103-1/4.
(39) Siwy, Z.; Heins, E.; Harrell, C. C.; Kohli, P.; Martin, C. R. *J. Am. Chem. Soc.* **2004**, *126*, 10850–10851.
(40) Stein, S.; Kruithof, M.; Dekker, D. *Phys. Rev. Lett.* **2004**, *93*, 035901.
(41) Vlassiouk, I.; Siwy, Z. S. *Nano Lett.* **2007**, *7*, 552–556.
(42) Kalman, E. B.; Vlassiouk, I.; Siwy, Z. S. *Adv. Mater.* **2008**, *20*, 293–297.
(43) Wanunu, M.; Meller, A. *Nano Lett.* **2007**, *7*, 1580–1585.
(44) Ali, M.; Mafé, S.; Ramírez, P.; Neumann, R.; Ensinger, W. *Langmuir* **2009**, *25*, 11993–11997.
(45) Ali, M.; Ramírez, P.; Mafé, S.; Neumann, R.; Ensinger, W. *ACS Nano* **2009**, *3*, 603–608.
(46) Ali, M.; Schiedt, B.; Healy, K.; Neumann, R.; Ensinger, W. *Nanotechnology* **2008**, *19*, 085713.
(47) Yameen, B.; Ali, M.; Neumann, R.; Ensinger, W.; Knoll, W.; Azzaroni, O. *Chem. Commun.* **2010**, *46*, 1908–1910.
(48) Yameen, B.; Ali, M.; Álvarez, M.; Neumann, R.; Ensinger, W.; Knoll, W.; Azzaroni, O. *Polym. Chem.* **2010**, *1*, 183–192.
(49) Yameen, B.; Ali, M.; Neumann, R.; Ensinger, W.; Knoll, W.; Azzaroni, O. *Nano Lett.* **2009**, *9*, 2788–2793.
(50) Yameen, B.; Ali, M.; Neumann, R.; Ensinger, W.; Knoll, W.; Azzaroni, O. *J. Am. Chem. Soc.* **2009**, *131*, 2070–2071.
(51) Ariga, K.; Hill, J. P.; Ji, Q. *Phys. Chem. Chem. Phys.* **2007**, *9*, 2319–2340.
(52) Decher, G. In *Multilayer Thin Films*; Decher, G., Schlenoff, J. B., Eds.; Wiley-VCH: Weinheim, Germany, 2002; Chapter 1, pp 1−46.
(53) Shia, X.; Shen, M.; Möhwald, H. *Prog. Polym. Sci.* **2004**, *29*, 987–1019.
(54) Bertrand, P.; Jonas, A. M.; Laschewsky, A.; Legras, R. *Macromol. Rapid Commun.* **2000**, *21*, 319–348.
(55) Ariga, A.; Ji, Q.; Hill, J. P.; Vinu, A. *Soft Matter* **2009**, *5*, 3562–3571.
(56) Steinhart, M. *Adv. Polym. Sci.* **2008**, *220*, 123–187.

materials inside nanopores. The incorporation of polyelectrolyte multilayers inside nanoporous templates has led to the generation of polymeric tubular structures with complex but well-controlled wall morphologies as well as to the construction of hybrid membranes with tailored gating properties.[57−61] Since the size of the supramolecular building blocks is commensurate with the nanostructure dimensions, they can exhibit a completely different physical behavior owing to nanoconfinement-driven topological changes. For instance, recent work by Jonas and co-workers revealed very interesting features regarding the nanoconfined supramolecular organization of polyelectrolyte multilayers.[62] When LbL assembly is performed within nanopores, a very different picture emerges and, in contrast to that observed on planar surfaces, no significant dependence of the thickness on the molar mass or the ionic strength is observed. Because of the diversity of functional properties and the relative ease of preparation owing to simple experimental protocols, LbL polyelectrolyte assemblies can be viewed as perhaps the most straightforward approach to manipulating the surface charge of single solid-state asymmetric nanopores.

In spite of its relevance, the use of LbL assemblies as building blocks to manipulate the rectification properties of asymmetric nanopores remains completely unexplored. Successful integration of supramolecularly organized polyelectrolyte multilayers as key elements regulating the ionic transport through asymmetric nanopores relies on a thorough understanding of the functional properties of these systems confined into fluidic structures with dimensions down to a few nanometers. We have described here the first example of single solid-state asymmetric nanopores functionalized with layer-by-layer assemblies of polyelectrolytes. Studying supramolecular organization inside single nanopores poses several analytical challenges due to the very small sample size. Hence, substantial theoretical attention has been directed toward the transport properties of asymmetric nanopores modified with these supramolecular assemblies.

Our experimental and theoretical findings revealed that the construction of LbL polyelectrolyte multilayers inside nanopores constitutes an interesting example of how nanoconfinement affects the functional features of supramolecular architectures as a result of the reduction of the dimensionality of the system. The characteristics of the surface-charge-governed ionic transport through asymmetric solid-state nanopores, modified with supramolecular polyelectrolyte assemblies, were found to depend highly on the number of layers assembled on the pore wall. The rectifying properties and surface charge density of the asymmetric nanopores decrease dramatically with the number of PAH/PSS grown inside the nanopore. This was attributed to the structural reorganization of the polyelectrolyte layer that leads to the efficient formation of bulk ion pairs within the film and consequently promotes a marked decrease in the net fixed charges on the nanopore walls. We consider this work has

profound implications not only for the molecular design of nanofluidic elements using supramolecular architectures but also for understanding the predominant role of nanoconfinement effects in dictating the functional properties of physically constrained soft matter based systems.

Experimental Section

Materials. Polymer foils of polyethylene terephthalate (PET) (Hostaphan RN 12, Hoechst) of 12 μm thickness were irradiated at the linear accelerator UNILAC (GSI, Darmstadt) with single swift heavy ions (Pb, U, and Au) having an energy of 11.4 MeV per nucleon. Poly(allylamine hydrochloride) (PAH, MW ∼15 000) and poly(sodium 4-styrenesulfonate) (PSS, MW ∼70 000) were obtained from Sigma-Aldrich, Germany. The surfactant Dowfax* 2A1 (Dow Chemical) was used as received without further purification.

Fabrication of Asymmetric Nanochannels. The fabrication of a single asymmetric nanochannel in a PET membrane was accomplished by asymmetric surfactant-controlled etching of the damage trail of a single heavy ion which passed through this membrane. Briefly, a heavy ion irradiated membrane was treated with soft UV light (the UV source provides ∼1.5 and 4 W m^{-2} of the electromagnetic power of wavelength in the ranges 280−320 and 320−400 nm, respectively) for 35 h from one side only. Then the membrane was placed in a conductivity cell in which it served as a dividing wall between the two compartments. The pure etchant (6 M NaOH) was filled on the UV-sensitized side, while the other half of the cell, adjoining the non-UV-treated side of the membrane, was filled with protecting solution (6 M NaOH + 0.04% v/v surfactant). The etching process was carried out at 60 °C. During the etching process, a potential of −1 V was applied across the membrane in order to observe the current flowing through the nascent nanopore. The current remains zero as long as the channel is not yet etched through, and after the breakthrough an increase of current is observed. The etching process was stopped when the current was reached at a certain value and the channel was washed first with 1 M HCl in order to neutralize the etchant, followed with deionized water. After etching, the diameter (D) and consequently the radius of the large opening (a_R) of the channel was determined by field emission scanning electron microscopy (FESEM) using a PET sample containing 10^7 pores/cm^2 which was etched simultaneously with the single channel under the same conditions. Then, as a first approximation, the diameter of the small opening (d, $d = 2a_L$, see Figure 1c,d) was estimated by assuming the conical geometry of the channel from its conductivity using the relation

$$d = 4LI/\pi D\kappa V$$

where L is the length of the pore which could be approximated to the thickness of the membrane, d and D are the small and large opening diameters of the channel, respectively, κ is the specific conductivity of the electrolyte, V is the voltage applied across the membrane, and I is the measured current.

Layer-by-Layer (LbL) Self-Assembly of PAH and PSS. Aqueous solutions of poly(allylamine hydrochloride) (PAH) and poly(styrene sulfonate) (PSS) were each prepared with a concentration of 1 mg/mL. A polymer membrane containing a single asymmetric nanochannel was mounted in the conductivity cell. The halves of the cell were filled with the solution of polycation (PAH) for 2 h. After the adsorption of electrolyte, the membrane with the positively charged channel was washed with distilled water, and the $I−V$ curve was measured using unbuffered 0.1 M KCl (pH ∼6.0) as an electrolyte for the examination of successful adsorption. Then the solution of polyanions (PSS) was introduced on both sides of the positively charged channel and allowed to adsorb electrostatically for a further 2 h. Similarly, after washing with water, the $I−V$ curve was measured. By using the same procedure, other

(57) Ai, S.; Lu, G.; He, Q.; Li, J. *J. Am. Chem. Soc.* **2003**, *125*, 11140–11141.
(58) Liang, Z.; Sucha, A. S.; Yu, A.; Caruso, F. *Adv. Mater.* **2003**, *15*, 1849–1853.
(59) Savariar, E. N.; Krishnamoorthy, K.; Thayumanavan, S. *Nat. Nanotechnol.* **2008**, *3*, 112–117.
(60) Hong, S. U.; Malaisamy, R.; Bruening, M. L. *Langmuir* **2007**, *23*, 1716–1722.
(61) Lee, D.; Nolte, A. J.; Kunz, A. L.; Rubner, M. F.; Cohen, R. E. *J. Am. Chem. Soc.* **2006**, *128*, 8521–8529.
(62) Alem, H.; Blondeau, F.; Glinel, K.; Demoustier-Champagne, S.; Jonas, A. M. *Macromolecules* **2007**, *40*, 3366–3372.
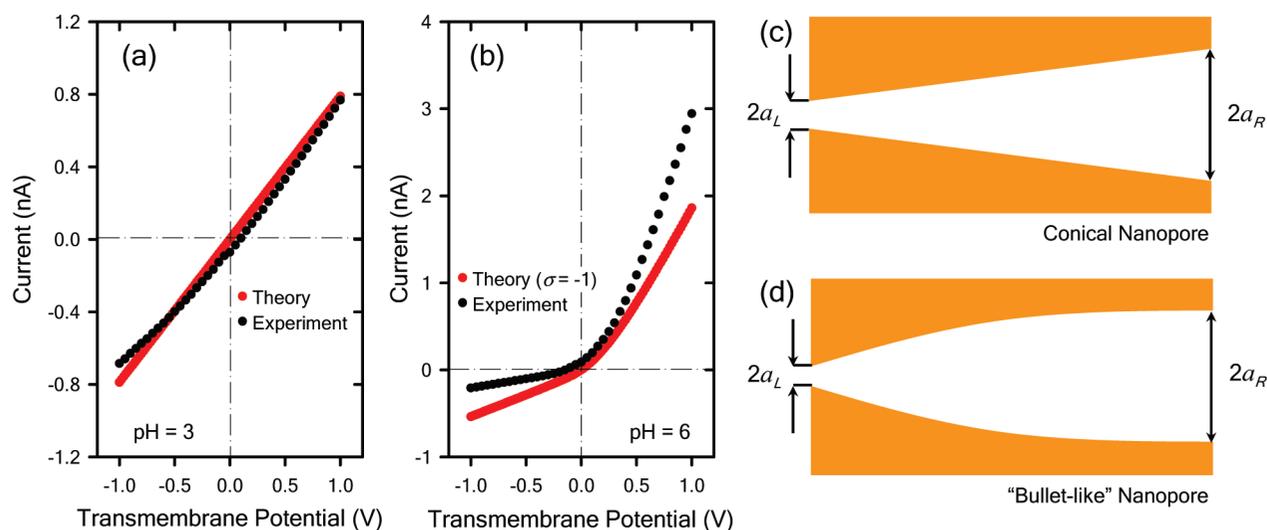
Figure 1. (left) $I-V$ characteristics of a single conical nanopore in a PET membrane recorded in 0.1 M KCl under different pH conditions: (a) pH 3, (b) pH 6. The black and red symbols indicate the experimental values and the theoretical results from a PNP model assuming a conical nanopore shape, respectively. The surface charge density (σ) is expressed in e/nm^2. (right) Schematic representation describing the geometric features of (c) conical and (d) bulletlike nanopores.

alternative layers of PAH/PSS were also electrostatically deposited inside the channel.

Results and Discussion

Single asymmetric nanopores were fabricated by irradiation of polyethylene terephthalate (PET) films with accelerated heavy ions, followed by chemical etching of the latent ion tracks: i.e., the so-called "track-etching technique".[27] Generally speaking, these pores have the shape of a tapered cone that is characterized by two openings having markedly different diameters. As discussed above, such nanopores rectify the current if the pore walls have excess surface charge.[21,39] The sign of the surface charge controls which ions pass through the pore as well as the direction of rectification. Hence, nanopores with negative surface charge (like the as-synthesized nanopores) are cation selective and rectify such that the preferential direction of cation flow is from the small opening toward the large opening of the nanochannels. A major challenge in nanotechnology is the incorporation of theoretical tools providing and describing a realistic scenario capable of revealing new insights into the physical phenomena taking place in restricted geometries. Theoretical modeling using a continuum approach based on the Nernst−Planck equations in particular have provided a solid conceptual framework for describing the experimental $I-V$ curves, estimating realistic values of parameters that are difficult to characterize experimentally (e.g. nanopore surface charge density), and understanding the complex nature of the processes occurring inside the nanopore.[37,45] Hence, prior to studying the LbL assembly of polyelectrolytes, we proceeded to describe the experimentally observed rectification behavior of the as-synthesized carboxylate-terminated asymmetric nanopores in terms of a continuous model based on the Poisson-Nernst−Planck (PNP) formalism.[37] The basic equations describing the transport through the nanopore are the Nernst−Planck equations

$$\vec{J}_i = -D_i(\nabla c_i + z_i c_i \nabla \phi) \quad i = \text{K}^+, \text{Cl}^- \tag{1}$$

the Poisson equation

$$\nabla^2 \phi = -\frac{F^2}{\varepsilon R T} \sum_i z_i c_i \tag{2}$$

and the continuity equation

$$\nabla \cdot \vec{J}_i = 0 \tag{3}$$

where $\vec{J}_i$, c_i, D_i, and z_i are the flux, the local concentration, the diffusion coefficient, and the charge number of ion i (i = K$^+$, Cl$^-$), with ϕ and ε being the local electric potential (in RT/F units) and dielectric permittivity of the solution within the pore, respectively.

Numerical integration of eqs 1−3 provides the concentration profiles of mobile ions $c_i(x)$ and the electric potential $\phi(x)$ at a given applied voltage. In our case we used the approximated method described in refs 37 and 63. Once these profiles have been determined, the ionic fluxes J_i are obtained using eq 1. From the ionic fluxes, the total electric current passing through any arbitrary section of the nanopore is then calculated. Digital simulations were performed using Mathematica and a combination of shooting and relaxation methods in order to solve the resulting two-point boundary value problem.

A quantitative comparison of theoretical and experimental results first requires the estimation of the nanopore dimensions. The radius of the wide pore opening is determined by field emission scanning electron microscopy, using a polymer foil containing ~10^7 pores/cm^2. This sample was etched simultaneously with the PET foil containing a single pore under the same conditions.[45] Then, the radius of the pore tip was calculated from the (linear) fitting of the $I-V$ curve for the uncharged nanopore: i.e., pH 3 (Figure 1a). The values obtained in our case were $a_R = 110$ nm and $a_L = 18$ nm. Thereafter, we tried to fit the experimental $I-V$ curve of the as-synthesized pore measured at pH 6, assuming a conical geometry in the channel architecture.

Under these conditions the PET films are negatively charged, bearing anionic carboxylate groups. The only free parameter

(63) Ramírez, P.; Apel, P. Y.; Cervera, J.; Mafé, S. *Nanotechnology* **2008**, *19*, 315707.

of the model is the surface charge σ (in elementary charges per square nanometer). As can be observed, the experimental rectified current is significantly higher than that obtained from the theoretical description, thus resulting in a mismatch between the experiments and the estimated ionic current using realistic σ values in the calculations (Figure 1b). This can be attributed to the fact that the shape of the pore might not be exactly conical.

As is well known, the region of the small opening greatly influences the $I-V$ characteristics of the nanopores. Therefore, we have assumed that the pore slightly deviates from a conical shape (Figure 1c,d). Recent work by Ramírez et al. describes in detail the critical role of the tip geometry in determining its rectification properties.[63] In this model, the pore radius a at a point of coordinate x along the pore axis is given by

$$a(x) = \frac{a_R - a_L \exp[-(d/h)^n] - (a_R - a_L)\exp[-(x/d)^n(d/h)^n]}{1 - \exp[-(d/h)^n]} \quad (4)$$

where the pore geometry is controlled by the parameters n and d/h. A variety of shapes and dimensions found experimentally can be reproduced using eq 4. For $n = 1$ and $d/h > 0$ pore profiles showing concave, bulletlike pore tips are obtained (the limit $d/h \rightarrow 0$ gives a conical pore).[3,4,28] As d/h increases while keeping $n = 1$, the region of the lumen becomes longer and the pore tip gets more tapered. For $d/h \rightarrow 0$ and $n > 1$ pore profiles with convex, trumpet-like pore tips, similar to those seen in refs 2, 3, and 28. As n increases, the narrow region close to the pore tip becomes longer. For $d/h > 0$ and $n > 1$ pore tips and lumens of variable length are obtained. Previous results reveal that pores with concave bulletlike tips display rectification efficiencies higher than those that are exactly conical.[63] In contrast, the rectification ratios showed by pores with convex, trumpet-like tips are noticeably lower than those characteristic of conical pores. In our case, the experiments show that the rectified currents are only slightly higher than those corresponding to conical pores. Therefore, the pore geometry should not depart too much from the conical shape. We have chosen $n = 1$ and $d/h = 2-4$ in the calculations. These values lead to pores with slightly tapered bulletlike tips (Figure 1c,d). The results obtained from modeling the experimental $I-V$ curve considering a negatively charged (pH 6) asymmetric nanopore with a bullet-type tip are described in Figure 2. The simulated $I-V$ representations of nanopores with bulletlike tips revealed a remarkable improvement in the theoretical description of the experimental results. From the fitting of the $I-V$ curves at pH 3 (uncharged pores) (not shown) different tip radii were obtained from the different d/h conditions. They corresponded to $d/h = 2$ ($a_L = 9.5$ nm), $d/h = 3$ ($a_L = 7$ nm), and $d/h = 4$ ($a_L = 5.5$ nm).

On characterizing the nanopore, we proceeded to its surface modification via consecutive layer-by-layer adsorption of poly-(allylamine hydrochloride) (PAH) and poly(styrenesulfonate) (PSS) on the pore surface (Figure 3). Initially, the as-prepared polymer membrane containing the carboxylate-functionalized single asymmetric nanochannel was mounted in the conductivity cell and the halves of the cell were filled with the polycation solution (PAH, 1 mg/mL) for 2 h. After careful rinsing with distilled water, the $I-V$ curve of the $(PAH)_1(PSS)_0$-modified pore was measured using 0.1 M KCl (pH ~6.0) as electrolyte.

As expected, the adsorption of PAH reverted the permselective characteristics of the nanopore and consequently the $(PAH)_1(PSS)_0$-modified pore displayed well-defined rectifying,
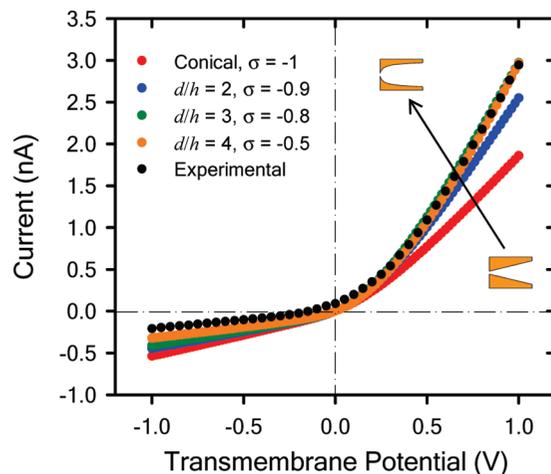

Figure 2. Experimental $I-V$ curve of the carboxylate-functionalized PET nanopore (●) (pH 6) and the corresponding theoretical fittings (different colors) assuming several bulletlike tip shapes. The electrolyte was 0.1 M KCl. The surface charge density (σ) is expressed in e/nm².

anion-selective properties (Figure 4a). Then, the polyanion solution (PSS) was introduced on both sides of the $(PAH)_1(PSS)_0$-modified pore and was allowed to adsorb electrostatically for a further 2 h. Similarly, after washing with water, the $I-V$ curve was measured (Figure 4b). The following alternate PAH/PSS layers were assembled using the same procedure. It is worth mentioning that the successive assembly of polyelectrolyte layers on the pore surface will reduce the pore radii. This is an important factor that was taken into account during the $I-V$ simulations. In accordance with recent experimental data reported by Zykwinska et al.,[64] we have assumed that in our case each assembled polyelectrolyte layer will reduce the pore radii by 0.5 nm (higher reductions would eventually close the pore tip in the cases $d/h = 3, 4$, in contrast to our observations).

Figure 4a shows the theoretical fittings for the case of the nanopore functionalized with the first PAH layer. We have assumed a reduction of 0.5 nm in both a_L and a_R in all the geometries considered. It is evident that the theoretical curves fit nicely the experimental data for $d/h = 2-4$ using the same absolute values for σ as in Figure 3: i.e., a carboxylate-modified pore. This indicates that the adsorption of the first layer of PAH on the COO^--terminated pore reverses the sign of the fixed charges while the number of fixed charges on the pore walls is kept constant. The fitting of the experimental values obtained for the PSS assembly on the $(PAH)_1(PSS)_0$-modified pore is depicted in Figure 4b. We see now that, in order to fit the experiments, the absolute values of σ must be reduced significantly with respect to their absolute values in the previous layer. With this assumption, the calculations fit nicely the experimental $I-V$ curves, especially in the cases $d/h = 2-4$.

In order to gain more insight into the role of the polyelectrolyte assembly as a key element in determining the pore surface charge and its subsequent influence on the nanopore rectifying properties, we have simulated the $I-V$ curves for the successive polyelectrolyte layers. The results are shown in Figure 5 and are consistent with the trends described above: when a PAH layer is assembled onto a PSS layer, the asymmetric nanopore displays anion-selective properties and, conversely, PSS-terminated assemblies confer cation-selective

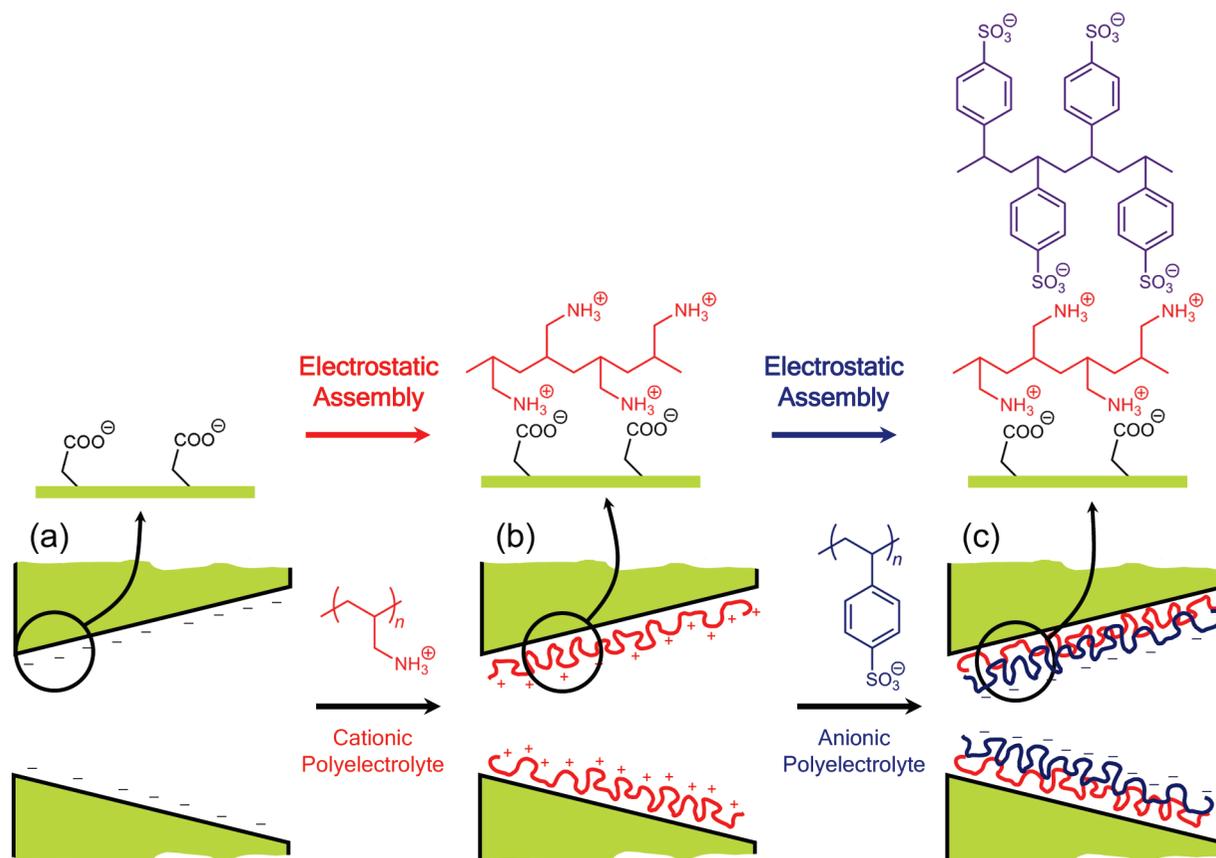(64) Zykwinska, A.; Radji-Taleb, S.; Cuenot, S. *Langmuir* **2010**, *26*, 2779–2784.

Figure 3. Illustrative schematic of the sequential nanopore modification via layer-by-layer assembly of polyelectrolytes: (a) as-synthesized nanopore; (b) $(PAH)_1(PSS)_0$-modified nanopore; (c) $(PAH)_1(PSS)_1$-modified nanopore.

properties to the nanofluidic device. It can be also observed that for nanopores modified with seven or eight polyelectrolyte layers, the results calculated for $d/h = 3, 4$ deviate noticeably from the experimental $I-V$ curves. Thus, it seems that the pore geometry that more accurately describes our experimental results is the case $d/h = 2$ (Figure 6), which corresponds to a bulletlike nanopore that slightly deviates from the typical conical shape. In the case of the first PAH layer assembled on the carboxylate-modified PET nanopore, the theoretical curve fits the experimental points using the same value of σ (in absolute value) as in the previous (substrate) layer. This indicates that charge reversal operates as commonly observed in multilayer growth on planar surfaces. The key to attain polyelectrolyte multilayer propagation is surface charge reversal. The polyelectrolyte adsorption may lead to a charge greater than that of the bare surface, so that the overall surface–polyelectrolyte complex has a charge opposite to that of the substrate. This phenomenon is known as surface charge *overcompensation*. When the overcharging is large enough to completely reverse the bare surface charge, the resulting charge surplus of the complex can be used to attract a second type of polyelectrolyte having a charge opposite to that of the first polyelectrolyte layer. This mechanism, by which each deposition step leaves the surface primed for the next immersion in the oppositely charged polymer, is an essential requirement for polyion multilayer assembly.[52]

However, the incorporation of PSS on the $(PAH)_1(PSS)_0$-terminated assembly leads to a decrease in the absolute value of σ in the pore walls from 0.9 to 0.3 e/nm². Further estimation of the surface charges after sequential assembly of PAH and PSS layers revealed an intriguing feature of the nanopore-confined LbL assembly. The surface charge used in the

calculations had to be reduced significantly from the values employed in the previous layer in order to fit the experiments. The variation of σ as a function of the multilayer assembly clearly illustrates a decreasing trend upon increasing the number of polyelectrolyte layers (Figure 7). Furthermore, the Figure 7 plot also describes an interesting finding: when a PAH layer is adsorbed onto a PSS layer, the theoretical curves fit the experimental points using the same value of σ as in the previous layer; however, when a PSS layer is adsorbed on a PAH layer, the absolute value of σ used in the calculations must be reduced from the values employed in the previous layer in order to fit the experiments. The theoretical calculations indicate that the multilayer growth promotes a marked decrease in the effective surface of the charged pore walls. This theoretical assertion is strongly supported by the very marked diminution of the rectification properties of the nanofluidic element upon increasing the number of PAH/PSS layers. The rectification efficiency (f_{rec}) is an experimental parameter that describes the permselective properties of the nanopore (current rectification) and is defined as the absolute value of the current ratio I(on state)/I(off state) at a given voltage (± 1 V).

As is well known, f_{rec} is sensibly correlated with the nanopore surface charge (σ), and consequently a slight increase/decrease in σ can trigger a marked increase/decrease in f_{rec}. From Figure 7 we can unambiguously conclude that, regardless of the exact pore geometry (bulletlike or conical), the successive growth of polyelectrolyte multilayers renders the pore walls less charged. Or, in other words, *the overcompensation vanishes during multilayer growth*.

Charge reversal upon sequential adsorption of PAH and PSS on planar surfaces and colloidal particles has been extensively
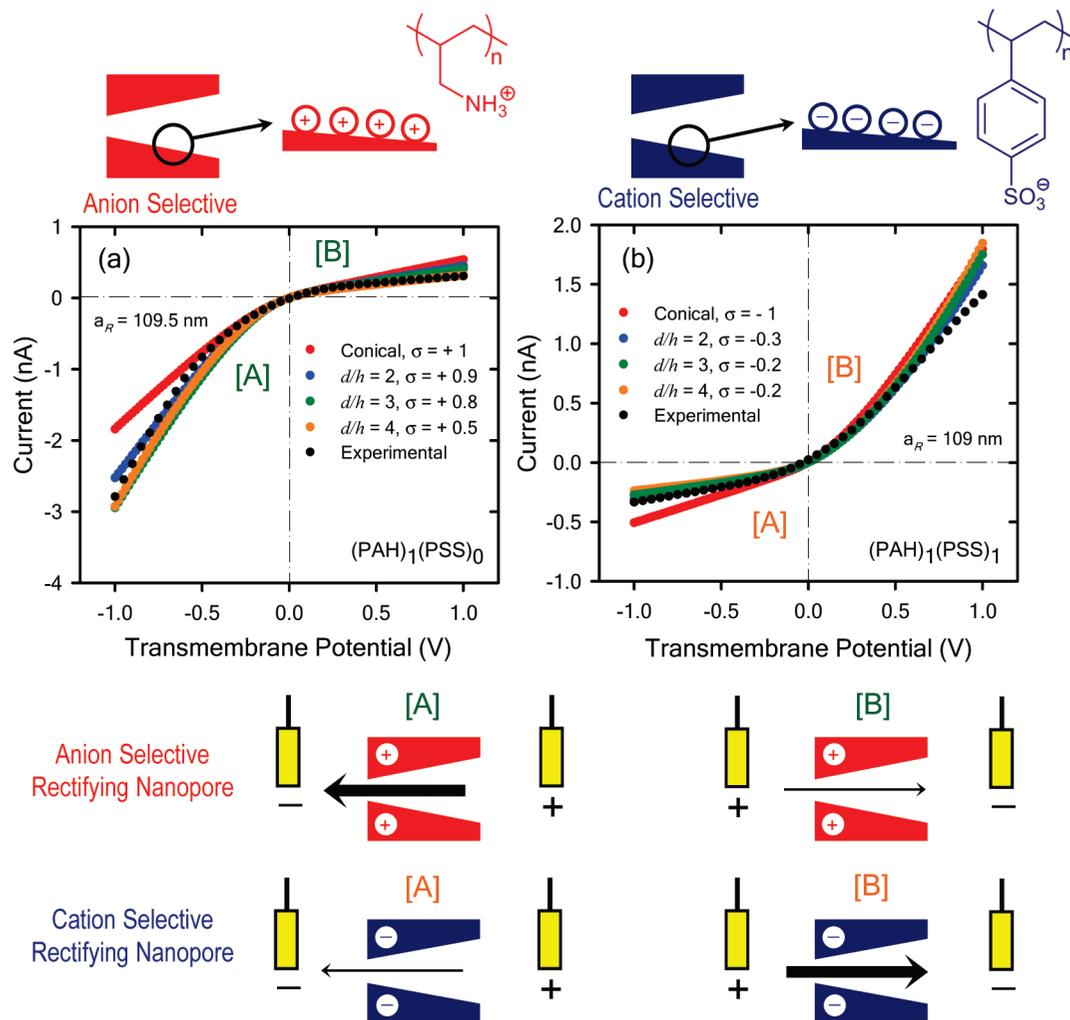
Figure 4. Experimental $I-V$ curves (●) corresponding to (a) $(PAH)_1(PSS)_0$-functionalized PET nanopore (anion selective) and (b) $(PAH)_1(PSS)_1$-functionalized PET nanopore (cation selective). The experimental plots include the corresponding theoretical fittings (different colors) assuming several bulletlike tip shapes and surface charge conditions. The surface charge density (σ) is expressed in e/nm². The figure also describes the chemical structure of the polyelectrolyte constituting the topmost layer of the supramolecular assembly. The illustration at the bottom of the figure indicates the preferential ion flux through $(PAH)_1(PSS)_0$ (red) and $(PAH)_1(PSS)_1$ (blue) modified conical nanopores under different polarization conditions ([A] and [B]). The arrows indicate the direction of the electric current under the applied potential and, therefore, always point in the direction of the movement of positive ions. Thick (thin) arrows indicate the direction of the current in the high (low) conductance state. The current−voltage curves of the nanopores are dictated mainly by the properties of the pore tip, which is the part of the nanopore with lower electric resistance. If the pore is positively charged, the high conductance state is obtained when the majority carriers (anions) enter first the nanopore tip and therefore find the lower resistance. This corresponds to $V < 0$ according to our sign criteria. On the other hand, if the pore is negatively charged, the high conductance state is found again when the majority ions (cations) enter first the nanopore tip. This occurs now for $V > 0$.

reported in the literature.[65,66] Negative ζ potentials were observed when PSS was the outer layer, and positive ζ potentials were measured for PAH as the outer layer in colloidal particles modified with these multilayered films. The alternating ζ potential ($\pm 40-50$ mV) with layer number evidence the charge reversal during the stepwise PSS/PAH multilayer growth. The stark contrast between PAH/PSS multilayer systems, grown on planar surfaces and inside nanopores, suggests the emergence of interfacial and geometric-confinement effects, with strong implications for the molecular design of ionic rectifiers as well as for the construction of soft nanomaterials through the electrostatic assembly of charged macromolecular building blocks in confined environments. This would indicate that the typical scenario describing the electrostatic assembly on planar

surfaces cannot be straightforwardly extrapolated to nanopores. For example, it has been demonstrated that the electrostatic assembly of charged dendrimers and polyanions on planar sustrates is feasible and charge reversal is accomplished during the multilayer growth.[67] However, recent work by Savariar et al. indicates that this situation is no longer applicable within a nanopore.[68] Upon assembling polypropyleneimine (PPI) dendrimers (second generation, G2, containing eight amino surface groups) on poly(acrylic acid) (PAA) modified nanopores, the diameter was reduced from 28 to 23 nm. Since the positively charged PPI dendrimers decorated the pore walls, it was expected that the anionic probe calcein would diffuse through the pores more rapidly than the cationic rhodamine 6G. Control experiments revealed no observable differences in the diffusion rates of both probes and, more importantly, no differences were observed after comparing the diffusion of both dyes through

(65) Caruso, F.; Lichtenfeld, H.; Donath, E.; Möhwald, H. *Macromolecules* **1999**, *32*, 2317–2328.
(66) Lowack, K.; Helm, C. A. *Macromolecules* **1998**, *31*, 823–833.

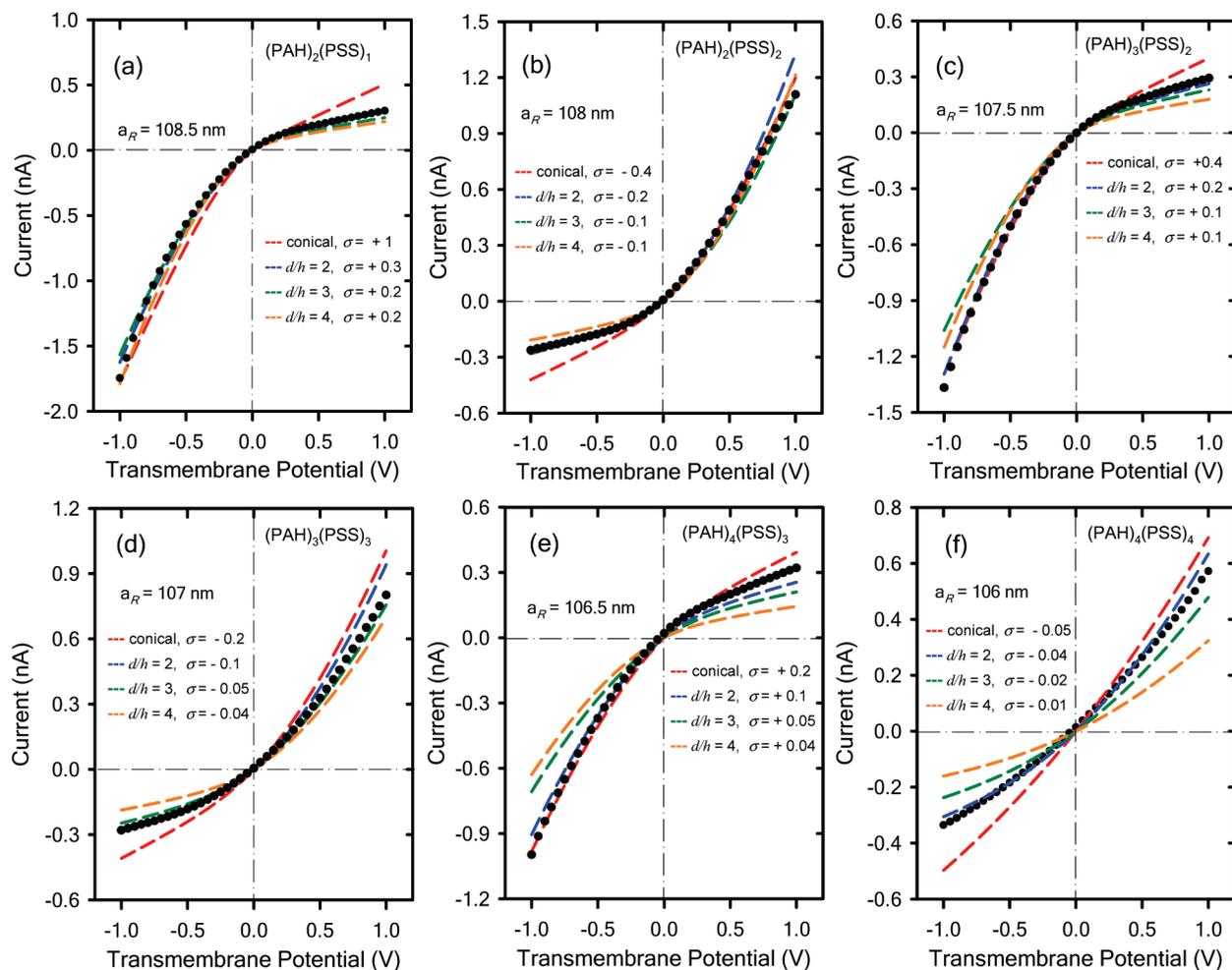(67) Khopade, A. J.; Caruso, F. *Nano Lett.* **2002**, *2*, 415–418.

Figure 5. Experimental I−V curves (●) recorded in 0.1 M KCl corresponding to single asymmetric nanopores modified with different polyelectrolyte assemblies: (a) $(PAH)_2(PSS)_1$; (b) $(PAH)_2(PSS)_2$; (c) $(PAH)_3(PSS)_2$; (d) $(PAH)_3(PSS)_3$; (e) $(PAH)_4(PSS)_3$; (f) $(PAH)_4(PSS)_4$. The experimental plots include the corresponding theoretical fittings (different colors) assuming several bulletlike tip shapes and surface charge conditions. The surface charge density (σ) is expressed in e/nm^2.
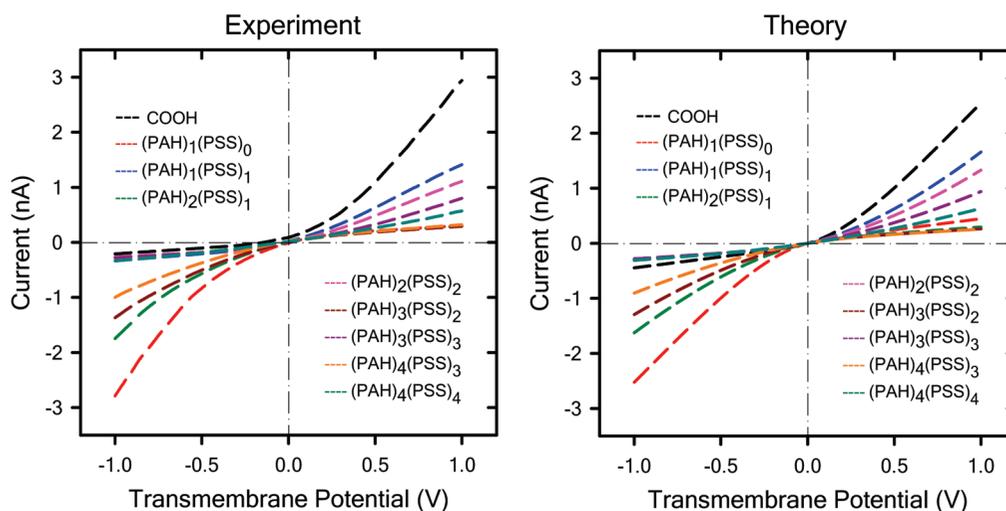

Figure 6. Experimental I−V curves (left) of the single asymmetric nanopore modified with an increasing number of (PAH)(PSS) assemblies and the theoretical results from the PNP model (right) assuming an asymmetric nanopore displaying a bulletlike tip shape ($d/h = 2$). The electrolyte was 0.1 M KCl.

PPI-G2/PAA-modified and unfunctionalized pores. It is worth indicating that diffusion of rhodamine 6G was faster than that of calcein in PAA-modified nanopores. This suggests that PPI-G2 dendrimers have essentially neutralized the negative charge

of PAA; however, they were not able to provide the pore walls with an overall positive charge: i.e., no charge reversal.

If we consider the critical role played by charge overcompensation in the construction of electrostatic supramolecular
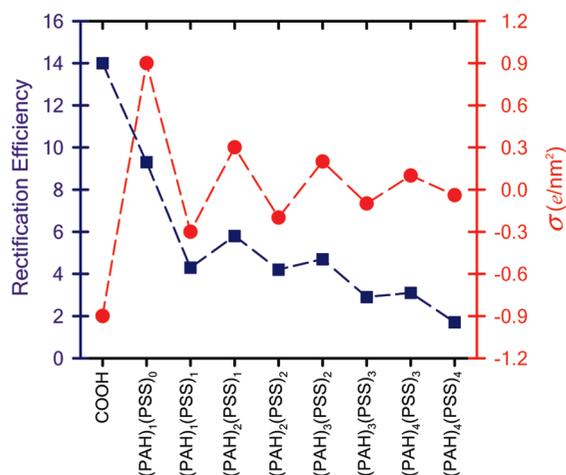
Figure 7. Representation of the rectification efficiency (■, in dark blue) (obtained from the experimental I−V curves) and the nanopore surface charge density (●, in red) (obtained from the theoretical fittings) as a function of the number of layers in the polyelectrolyte assembly. Lines have been drawn to guide the eye.

assemblies, one key question comes to light: why is the charge reversal mechanism no longer operating in the nanoscale pore?

To answer this question, we need to consider the basic mechanisms that govern the assembly of the polyelectrolyte multilayers.[52,54] It is generally assumed that the outermost layer, and not the underlying film, determines the surface potential. However, Möhwald and co-workers, studying the electrophoretic mobility of polystyrene-modified latex particles, found that not only the top layer but also the layers underneath contribute to the particle mobility.[69] Furthermore, it is now well-established that polyelectrolyte multilayer films are not constituted of well-separated layers but show interpenetration over about four neighboring layers.[52] Hence, topological constraints may contribute to the layer formation as well as the formation of ion pairs.

Along these lines, Schlenoff and co-workers suggested a more refined picture of multilayer architecture involving excess polymer charge dispersed over several layers and not simply contained in the outer layer.[70−72] Taking this view, the bulk of the polyelectrolyte multilayer is *intrinsically* compensated, in contrast to the region near the surface in which the excess polymer charge is counterbalanced by small ions. Both polymers are interpenetrated, allowing excess polymer (charge) to be distributed into the multilayer. Even though the bulk multilayer could be stoichiometrically counterbalanced, the surface bears considerable excess charge (overcompensation) due to the conformation of the topmost polymer layer. The combination of trains, contacting the growing multilayer and the size of free loops into solution, determines to a great extent the degree of surface charge overcompensation. Hence, confinement-induced topological changes of the outermost layer may affect the excess surface charge.[72] Then, it is reasonable to assume that in LbL

assembly from pure water (as in our case) intrinsic charge compensation involving a 1:1 stoichiometry between positive and negative charges takes place. However, interesting findings from Riegler and Essler indicate that this idea does not univocally apply to the PAH/PSS system.[73] Floating PAH/PSS multilayers adsorbed to a negatively charged dimyristoylphosphatidic acid monolayer at the air/water interface were analyzed quantitatively with respect to the internal charge stoichiometry of the polyelectrolytes. The experimental results reported by these authors indicated that the charge stoichiometry of the polyelectrolytes is *not* 1:1 and the PAH charges overcompensate the PSS charges. Typically the amounts of PAH exceeded those of PSS by more than 50% and in some cases by even 100% (at high ion concentrations). This means that the multilayers contain additional small counterions for complete charge compensation. Due to the higher amount of PAH monomers compared to PSS, the overall charge becomes more and more positive for all polyelectrolyte and ion concentrations. Furthermore, fluorescence studies performed on PAH/PSS multilayers preadsorbed on particle surfaces have provided unambiguous evidence that the outermost layers of the PAH/PSS assemblies contain positive binding sites represented by cationic groups of PAH which did not take part in the ion-pair formation multilayer growth.[65] In a similar fashion, surface force apparatus measurements indicated that on adsorption of PSS onto a PAH monolayer only a third to a half of the positive point charges are neutralized with PSS monomers and the rest of the negatively charged monomer units dangle into the solution.[66]

Hence, this suggests that the overall surface charge of the nanopore walls is mainly determined by the interplay of two factors. First, the nonstoichiometric successive assembly of polyelectrolyte layers within the confined pore geometry may lead to an enrichment of surface-confined charges (within the multilayer assembly), counterbalancing and neutralizing the charge of the outermost layer. At this point, it is necessary to mention recent interesting findings reported by Adusimilli and Bruening.[74] These authors studied the LbL assembly of poly-(styrene sulfonate) (PSS)/poly(diallyldimethylammonium chloride) (PDADMAC) on flat surfaces and on nanoporous alumina. They found that for silicon-supported PSS/PDADMAC films, terminated with PSS, ζ potentials changed from negative to positive as the number of adsorbed bilayers increased. These changes in film properties also manifested dramatic effects on the ion transport properties of (PSS/PDADMAC)$_n$-modified alumina membranes. The Cl$^-$/SO$_4^{2-}$ selectivities of these membranes were higher than 30 with (PSS)$_4$(PDADMAC)$_4$ films but only 3 with (PSS)$_6$(PDADMAC)$_6$ films. These experiments eloquently illustrate a sharp variation of the electrostatic environment with the number of layers in the multilayer polyelectrolyte film. The electrostatic interactions in PSS/PDADMAC assemblies have been extensively characterized by Caruso et al. using fluorescence techniques.[65] The binding data of fluorescent anionic probes revealed that a minimum of 20−30% of the cationic charges of PDADMAC in the upper layers (∼9 layers) of the multilayer films did not take part in the ion-pair binding to PSS. Furthermore, they also found a linear increase in the bound probe amount with polyelectrolyte layer number, thus indicating that the nominal amount of uncompensated cationic sites is proportional to the multilayer thickness. This provides additional evidence that the actual electrostatic environment of the multilayer is highly dependent

(68) Savariar, E. N.; Sochat, M. M.; Klaikherd, A.; Thayumanavan, S. *Angew. Chem., Int. Ed.* **2009**, *48*, 110−114.

(69) Donath, E.; Walther, D.; Shilov, V. N.; Knippel, E.; Budde, A.; Lowack, K.; Helm, C. A.; Möhwald, H. *Langmuir* **1997**, *13*, 5294−5305.

(70) Schlenoff, J. B.; Ly, H.; Li, M. *J. Am. Chem. Soc.* **1998**, *120*, 7626−7634.

(71) Schlenoff, J. B.; Dubas, S. T. *Macromolecules* **2001**, *34*, 592−598.

(72) Schlenoff, J. B. In *Multilayer Thin Films*; Decher, G., Schlenoff, J. B., Eds.; Wiley-VCH: Weinheim, Germany, 2002; Chapter 4, pp 99−132.

(73) Riegler, H.; Essler, F. *Langmuir* **2002**, *18*, 6694−6698.

(74) Adusumilli, M.; Bruening, M. L. *Langmuir* **2009**, *25*, 7478−7485.

on the layer thickness. It is worth mentioning that no quantitative conclusions can be made from ζ potential values because this magnitude is not proportional to the charge density, since the surface is composed of charges arranged in a layer of finite thickness and, in addition, the ζ potential depends on the polyelectrolyte conformation at the surface.[69,75] However, the variation of ζ potential reported by Bruening et al. is fully consistent with the thickness-dependent enrichment of fixed cationic charges described by Caruso and co-workers.

Second, the nanopore confinement determines how far the outermost polyelectrolyte loops and tails dangle into the solution. The behavior of nanoconfined polymeric building blocks has become one of the central issues of nanoscience. In particular, spatially confined species experience enhanced intermolecular interaction, which results in highly cooperative phenomena.[76] For instance, in a physically confined environment, structural frustration[77] and confinement-induced entropy loss[78] can play dominant roles in determining molecular organization, which in turn governs the physical chemistry of supramolecular systems when they are confined in spaces comparable to their molecular dimensions. For example, physical nanoconfinement can induce complete mixing in polymer blends[79] or, in the case of polyelectrolytes, trigger the irreversible formation of ion pairs.[80] It is most likely that after assembly significant chain rearrangement occurs and nanoconfinement effects dominate both the degree of polymer interpenetration and chain mobility in the outer layer, which in turn determines the flexibility and local structure of the polyelectrolyte assembly. The results of a recent study point to further evidence that corroborates this scenario. Jonas and co-workers have demonstrated that the growth process in nanopores differs from the one on flat surfaces and explained this behavior with a model based on polyelectrolyte complexation in confined spaces. These authors found no significant dependence of the multilayer thickness on the molar mass of polyelectrolytes and on the ionic strength of the solutions, thus indicating that the size of the chains in the starting solutions is of little importance for the process. However, the thickness of the LbL assemblies showed a marked dependence on the pore diameter, being proportional to pore diameter at the nanoscale. In this latter case, the experimental results validate the idea that nanoconfinement effects govern the local topological features of the polyelectrolyte assembly.

A scenario consistent with our findings in LbL-modified asymmetric nanopores is one that contemplates the long-range coupling of structural and electrostatic changes arising from the nonstoichiometric assembly and the nanoconfinement effects. During the sequential nonstoichiometric assembly, the film develops surface-confined positive charges counterbalanced by small mobile counterions: i.e., Cl^-. These extra uncompensated positive charges are responsible for partially neutralizing the determinant effect of the topmost layer in the case of PSS-capped assemblies. Furthermore, the formation and size of free

loops in solution that determine the charge reversal are also affected by the topological constraints generated by the nanopore confinement. Hence, the increasing number of PAH/PSS layers inside the nanopore imposes increasing topological restrictions to the incoming polyelectrolyte layers which may dictate the compaction and mobility of the polymer chains. This picture is in complete agreement with the model proposed by Jonas et al. in which chains entangle during their passing through the pores, due to a local increase in concentration, resulting in a dense, amorphous gel-like layer. Along these lines, the sequential confinement polyelectrolyte layers may lead to film reorganization, exhibiting much greater interpenetration and having a strong impact on the formation of ion pairs (more efficient complexation). As a result, the strong confinement and the effective polyelectrolyte intermixing at a molecular level acts as a driving force leading to complete ion pairing: i.e., net fixed charges vanish during sequential assembly. This explains within a qualitative framework the trend observed in our experiments. When the film thickness is increased, structural reorganization and sequential generation of positive charges and ion pairs take place in the bulk multilayer.

The interplay between these processes has a profound impact on the charge overcompensation process taking place inside the nanopore, and as a result, the net surface charge decreases after increasing the number of layers in the LbL assembly. For instance, the surface charge and the rectification efficiency decrease from -0.9 to -0.04 e/nm^2 and from 14 to ~ 2, respectively, after four PAH/PSS bilayers are assembled on the pore walls. The presented results clearly point to the fact that the nanoconfinement-induced topological organization, experienced by the polyelectrolyte supramolecular assemblies, has marked effects on the ionic selectivity of the fluidic device. Our combined experimental–theoretical approach to the construction of supramolecular architectures inside constrained geometries eloquently illustrates how nanoconfinement can promote the emergence of unexpected functional features in soft matter based systems.

Conclusions

Research in nanotechnology has always fostered the combination of techniques, tools, and concepts from different disciplines. Here, we introduced for the first time a study describing the modification of single asymmetric solid-state nanopores via the supramolecular assembly of ultrathin polyelectrolyte multilayer films formed by the consecutive adsorption of oppositely charged macroions. Furthermore, in order to investigate the underlying physics behind the experimentally observed phenomena, we employed a theoretical framework based on the Nernst–Planck–Poisson formalism to represent the ion transport across the nanopores functionalized with the supramolecular assemblies. Currently available experimental techniques are not capable of estimating diverse physical parameters associated with functionalized single nanopores with dimensions down to a few nanometers. Along these lines, through the incorporation of theoretical and computational tools to complement the experiments, we were able to obtain relevant information about the electrostatic conditions inside the nanopores. We have used a nanopore model that quantitatively reproduces the $I-V$ response of the experimental systems and enabled a reliable description of pore geometry, tip dimension, and surface charge density. The properties of the nanoconfined supramolecular assemblies were found to depend highly on the number of polyelectrolyte layers assembled on the pore wall. For instance,

(75) Donath, E.; Budde, A.; Knippel, E.; Bäumler, H. *Langmuir* **1996**, *12*, 4832–4839.
(76) Ariga, K.; Vinu, A.; Ji, Q.; Ohmori, O.; Hill, J. P.; Acharya, S.; Koike, J.; Shiratori, S. *Angew. Chem., Int. Ed.* **2008**, *47*, 7254–7257.
(77) Lambooy, P.; Russell, T. P.; Kellogg, G. J.; Mayes, A. M.; Gallagher, P. D.; Satija, S. K. *Phys. Rev. Lett.* **1994**, *72*, 2899–2902.
(78) Wu, Y.; Cheng, G.; Katsov, K.; Sides, S. W.; Wang, J.; Tang, J.; Fredrickson, G. H.; Moskovits, M.; Stucky, G. D. *Nat. Mater.* **2004**, *3*, 816–822.
(79) Zhu, S.; Liu, Y.; Rafailovich, M. H.; Sokolov, J.; Gersappe, D.; Winesett, D. A.; Ade, H. *Nature* **1999**, *400*, 49–51.
(80) Azzaroni, O.; Trappmann, B.; van Rijn, P.; Zhou, F.; Kong, B.; Huck, W. T. S. *Angew. Chem., Int. Ed.* **2006**, *45*, 7440–7443.

we have observed that the rectifying properties and surface charge density of the asymmetric nanopores decrease dramatically with the number of PAH/PSS bilayers grown inside the nanopore. This was attributed to the structural reorganization and sequential generation of positive charges and ion pairs taking place in the bulk multilayer during the nanoconfined growth. The interplay between these processes has a profound impact on the charge overcompensation process taking place on planar assemblies. The experimental evidence reveals that nanoconfinement strongly affects the charge inversion process and that the nanopore surface charge decreases from -0.9 to -0.04 e/nm^2 after assembling four PAH/PSS layers on the pore walls. The experimental results eloquently illustrate that the formation of supramolecular polyelectrolyte assemblies inside nanopores significantly differs from typical polyelectrolyte multilayers grown on planar surfaces. The construction of supramolecular architectures inside nanopores constitutes a fine example of how nanoconfinement might lead to new structures and functional properties through the reduction of the dimensionality of the system.

We consider that these results not only are of practical relevance for the construction of supramolecular assemblies into constrained geometries, such as nanopores, nanopipets, or nanoelectrodes,[81−85] but also are of importance in the emerging field of "soft nanotechnology",[86−88] provided that nanoconfinement effects dictate the functional properties of LbL polyelectrolyte assemblies. Finally, it is worth mentioning that this field is just in its infancy, and it is likely that both new experimental and theoretical tools will be needed to gain further insight into the physical/chemical phenomena arising from supramolecular organization under nanoconfinement.

JA101014Y

(81) Fu, Y.; Tokuhisa, H.; Baker, L. A. *Chem. Commun.* **2009**, 4877–4879.
(82) Wei, C.; Bard, A. J.; Feldberg, S. W. *Anal. Chem.* **1997**, *69*, 4627–4633.
(83) Wen, L.; Hou, X.; Tian, Y.; Nie, F.-Q.; Song, Y.; Zhai, J.; Jiang, L. *Adv. Mater.* **2010**, *22*, 1021–1024.
(84) White, R. J.; Ervin, E. N.; Yang, T.; Chen, X.; Daniel, S.; Cremer, P. S.; White, H. S. *J. Am. Chem. Soc.* **2007**, *129*, 11766–11775.
(85) Wang, G.; Zhang, B.; Wayment, J. R.; Harris, J. M.; White, H. S. *J. Am. Chem. Soc.* **2006**, *128*, 7679–7686.
(86) Huck, W. T. S. *Mater. Today* **2008**, *11*, 24–32.
(87) Jones, R. A. L. *Faraday Discuss.* **2009**, *143*, 9–14.
(88) Whitesides, G. M.; Lipomi, D. J. *Faraday Discuss.* **2009**, *143*, 373–384.